

Diffusive Shock Acceleration in Radiation Dominated Environments

G. Vannoni^{1*}, S. Gabici², and F. A. Aharonian^{2,1}

¹ Max-Planck-Institut für Kernphysik, Saupfercheckweg 1, Heidelberg 69117, Germany;

² Dublin Institute for Advanced Studies, 31 Fitzwilliam Place, Dublin 2, Ireland.

Preprint online version: March 3, 2019

ABSTRACT

Context. Radio, X-ray and gamma-ray observations provide us with strong evidence of particle acceleration to multi-TeV energies in various astrophysical sources. Diffusive Shock Acceleration is one of the most successful models to explain the presence of such high energy particles.

Aims. We discuss the impact of inverse Compton losses on the shock acceleration of electrons which takes place in radiation dominated environments, i.e. in regions where the radiation energy density exceeds that of the magnetic field.

Methods. We perform a numerical calculation, including an energy loss term in the transport equation of accelerated particles.

Results. We discuss the implications of this effect on the hard X-ray synchrotron and gamma-ray inverse Compton radiation, produced by shock accelerated electrons in young Supernova Remnants in the presence of large radiation fields (e.g. in the Galactic Center). We also discuss possible implications of our results for clusters of galaxies and gamma-ray binaries.

Conclusions. We demonstrate that the inverse Compton losses of electrons, in the Klein-Nishina regime, lead to spectra of ultra-relativistic electrons which may significantly differ from classical Diffusive Shock Acceleration solution. The most prominent feature is the appearance of a pile up in the spectrum around the cutoff energy.

Key words. shock acceleration – radiation mechanisms: non-thermal

1. Introduction

Diffusive Shock Acceleration (DSA) is the most successful and widely accepted mechanism to explain the acceleration of cosmic rays in many astrophysical environments. Despite the fact that the basic physics of DSA is very robust and reasonably well understood (see Blandford & Eichler 1987 and Malkov & Drury 2001 for a review), some crucial issues still need to be addressed.

In its simplest, test-particle, approach the theory of DSA predicts an energy spectrum for the accelerated particles which is a featureless power law $f(p) \propto p^{-\alpha}$ up to a maximum energy where the spectrum cuts off. For strong, non-relativistic shocks, where the mechanism is believed to operate very efficiently, the slope of the spectrum below the cutoff converges to the canonical slope $\alpha = 4$, independently of the details of the acceleration.

The value of the maximum energy attained by particles is determined by the competition between the acceleration time and the shortest of the three time scales: *i*) particle escape time from the accelerator; *ii*) particle energy loss time and *iii*) age of the accelerator. Therefore, while the energy spectrum below the cutoff is almost universal, the spectral shape of the cutoff depends dramatically on both the details of the acceleration mechanism and the physical process determining the particle maximum energy. In the case of electrons, that we consider in this paper, the maximum energy is in most cases limited by radiative synchrotron and inverse Compton losses in the ambient magnetic and photon fields.

The missing piece of information in the model is the diffusion coefficient of particles close to the shock, which determines the acceleration rate. For a given diffusion coefficient,

the problem is well defined and can be solved once the value of the magnetic field and the spectrum of the ambient radiation are specified. Although there is some uncertainty about this coefficient, one can reasonably assume that, due to the high level of turbulence expected close to the shock, the mean free path of particles is of the order of their Larmor radius r_L . Under these circumstances diffusion proceeds close to the slowest possible (so-called Bohm) rate with diffusion coefficient $D \sim r_L c/3$.

Several approaches can be found in the literature to the problem of electron acceleration at shocks in presence of radiative losses. Bulanov & Dogiel (1979), Webb et al. (1984) and Heavens & Meisenheimer (1987) considered the case of a diffusion coefficient constant in momentum and space. Recently Zirakashvili & Aharonian (2007) solved numerically the problem for $D(p)$ with an arbitrary momentum dependence. All the above mentioned approaches are limited to the case of dominant synchrotron losses.

In this paper, we solve numerically the problem for a general form of both the diffusion coefficient and the energy loss rate. In particular, we focus on the case, never considered before, in which the accelerator is embedded in a strong radiation field, characterized by an energy density much bigger than the magnetic one. Under this circumstance, inverse Compton losses dominate over synchrotron losses and, at the highest energies, modifications to the electron spectrum are expected, with respect to the case of synchrotron/Thomson losses, due to the transition between Thomson and Klein-Nishina regimes. This, in turn, strongly affects the spectrum of the radiation emitted by accelerated particles. We calculate numerically the exact shape of the spectrum in the whole energy range and we show that in the case of Klein-Nishina losses the particle distribution at the shock

* IMPRS fellow - e-mail: Giulia.Vannoni@mpi-hd.mpg.de

has a broad cutoff, due to the shallow energy dependence of the loss rate. Another important effect of Klein-Nishina losses is to harden the downstream electron spectrum close to the maximum energy, leading to the formation of a pronounced pile up. Such a feature can be observed in the photon spectrum, in particular for the synchrotron emission. On the inverse Compton emission the effect is less pronounced due to the fact that the Klein-Nishina cross-section intervenes twice, in opposite direction, to harden the electron spectrum and to soften the photon one leading to an almost exact compensation.

We describe the details of our model in Section 2 and discuss the main characteristics of the calculation by applying it to an ideal example in Section 3. In Section 4 we then apply our results to several astrophysical environments where the radiation field energy density dominates, namely to supernova remnants located close to the Galactic Centre, shocks in binary systems and accretion shocks around massive clusters of galaxies. For these systems we evaluate the spectrum of the accelerated particles together with the spectra of both the emitted synchrotron and inverse Compton radiation. We summarize in Section 5. The presence of a strong pile up at the high energy end of the synchrotron spectrum is the most remarkable feature.

2. The Model

We consider a plane parallel shock, where the fluid moves (in the shock rest-frame) along the x axis from $-\infty$ far upstream, to $+\infty$ far downstream and the shock is located at $x = 0$. We assume the velocity of the shock to be non-relativistic.

The transport equation for the particles distribution function, including the presence of energy losses, reads:

$$\frac{\partial f(x, p, t)}{\partial t} + u \frac{\partial f(x, p, t)}{\partial x} - \frac{\partial}{\partial x} \left(D(x, p) \frac{\partial f(x, p, t)}{\partial x} \right) - \frac{p}{3} \frac{\partial u}{\partial x} \frac{\partial f(x, p, t)}{\partial p} - \frac{1}{p^2} \frac{\partial}{\partial p} (p^2 L(x, p) f(x, p, t)) = Q(x, p), \quad (1)$$

where $L(x, p) = -\dot{p}$ is the loss rate taken to be positive and $Q(x, p)$ is the injection term; u represents the bulk velocity of the plasma in the shock rest-frame. In the following we will assume that the diffusion coefficient in the up and downstream regions $D_{1,2}$ does not depend on x and has the functional form $D(p) = D_0 p^\beta$ (although any expression for $D_{1,2}(x, p)$ can be easily implemented in the code) and that injection happens at the shock surface as a delta function in energy:

$$Q(x, p) = Q_0 \delta(x) \delta(p - p_0).$$

The formulation is general so that it can be applied to both protons or electrons, plugging in the relevant energy loss channels, namely proton-proton and proton-gamma interactions, for the hadronic channel, and synchrotron and inverse Compton (IC) emission for the leptonic one. In this paper we study the acceleration of electrons undergoing synchrotron and inverse Compton losses, in the case when the IC is dominant. This is the case if acceleration takes place in a region where the energy density of the ambient radiation field exceeds the magnetic one: $U_{rad} \gg B^2/(8\pi)$. In particular we are interested in studying the effect produced on both the electron and the photon distributions when IC losses proceed in the Klein-Nishina regime, namely when $\epsilon E/(mc^2)^2 \geq 1$ with E being the electron energy, m the electron mass and ϵ the ambient photon's energy.

In the following we assume that the background radiation field is isotropic and that the background magnetic field is constant in the upstream and downstream region and the two are related by $B_2 = \xi B_1$, where ξ is the compression factor. In the following we assume $\xi = 1$ (pure parallel shock) in order to point out the results of our calculation with more clarity, but such an assumption can be completely relaxed.

2.1. Electron Spectra

We solve Eq. (1) using a finite difference numerical scheme, implicit in time to guarantee unconditional stability and explicit in momentum. Since we are ultimately interested in the equilibrium spectrum of particles, we run the code until the solution converges to its steady state (time independent) value.

To solve the problem we need to insert the boundary conditions at the shock and at upstream/downstream infinity. For the boundary at the shock we consider again Eq. (1) and integrate it between 0_- immediately upstream and 0_+ immediately downstream, obtaining:

$$\frac{1}{3}(u_1 - u_2)p \frac{\partial f_0}{\partial p} = D_2 \frac{\partial f_0}{\partial x} \Big|_2 - D_1 \frac{\partial f_0}{\partial x} \Big|_1 + Q_0 \delta(p - p_0) \quad (2)$$

where the subscript 1 refers to the upstream region and 2 to the downstream one. At $\pm\infty$ we set $f(x, p) = 0$.

It is convenient to introduce two dimensionless variables in place of p and x . The first variable is p/p^* , where p^* is a parameter that estimates the cutoff momentum for the electron distribution, evaluated imposing equilibrium between the momentum gain in one acceleration cycle:

$$\Delta p_{acc} = \frac{4p}{3} \frac{(u_1 - u_2)}{c} \quad (3)$$

and the momentum loss per cycle:

$$\Delta p_{loss} = L_1(p)\Delta t_1 + L_2(p)\Delta t_2 \quad (4)$$

where the mean residence time in the up and downstream regions is $\Delta t_{1,2} = 4D_{1,2}(p)/cu_{1,2}$ (see Webb et al. 1984).

For the spatial coordinate we operate a change of variable both up and downstream. To reduce the large range in $|x|$ from 0 to ∞ to one more numerically feasible, we use an exponential variable:

$$z = exp \left[-\frac{|x|}{x_0} \right], \quad (5)$$

where x_0 is a characteristic length scale. The new variable now conveniently ranges from 0 to 1. Except for energies close to the cutoff, the accelerated particles can propagate one diffusion length ahead of the shock. The situation is different downstream, where the maximum distance from the shock a particle can reach is determined by energy losses. Thus, a reasonable choice for the length scale x_0 is:

$$x_{0,1} = \frac{D_1(p)}{u_1} \quad (6)$$

and

$$x_{0,2} = u_2 \tau_L, \quad (7)$$

for upstream and downstream respectively. The energy loss time is given by $\tau_L = p/L(p)$.

Once the steady state solution $f(x, p)$ of Eq. (1) is found, we evaluate the total spectrum integrated over space, $F(p) = \int f(x, p) dx$, which is the quantity required to evaluate the radiation spectrum emitted in the shock region. It is worth mentioning that the steady state integrated spectrum, below the cutoff energy, follows a power law. In the downstream region, in case of Thomson cooling, the differential spectrum in momentum space has index $\delta = \alpha + 1 = 5$. Upstream the maximum distance from the shock a particle can travel is essentially its diffusion length, therefore, for Bohm-like diffusion, this results in $\delta = \alpha - 1 = 3$.

2.2. Photon Spectra

Once we have the electron spectrum we can calculate the spectra of the radiation emitted both via synchrotron and IC.

For synchrotron radiation the energy flux at an energy ϵ is given by:

$$\Phi(\epsilon) = \frac{\sqrt{3} B e^3}{h m c^2} \int p^2 dp F(p) K(\epsilon/\epsilon_c). \quad (8)$$

where $\epsilon_c = h \nu_c$ is the energy corresponding to the critical frequency $\nu_c = 3eBp^2/(4\pi m^3 c^3)$ and $K(\epsilon/\epsilon_c)$ is the emission produced by the single electron of momentum p , charge e and mass m ; h represents the Planck constant.

In our case $F(p)$ is the total electron spectrum integrated up and downstream. The exact expression for the kernel function $K(\epsilon/\epsilon_c)$ in the case of a turbulent magnetic field is derived in Crusius & Schlickeiser (1986). With several percent accuracy this can be approximated by the analytical expression obtained in Zirakashvili & Aharonian (2007):

$$K(\epsilon/\epsilon_c) = \frac{1.81 e^{-\epsilon/\epsilon_c}}{\sqrt{(\epsilon/\epsilon_c)^{-2/3} + (3.62/\pi)^2}}. \quad (9)$$

We adopt this simpler expression.

The inverse Compton energy flux for an isotropic distribution of soft photons $n(\epsilon')$ upscattered by a population of electrons with spectrum $F(p)$ is (Blumenthal & Gould 1970):

$$\Phi(\epsilon) = \frac{2\pi e^4 \epsilon}{c} \int dp F(p) \int \frac{n(\epsilon') d\epsilon'}{\epsilon'} \left[2q \ln q + (1 + 2q)(1 - q) + \frac{1}{2} \frac{\epsilon^2}{pc(pc - \epsilon)} (1 - q) \right], \quad (10)$$

where

$$q = \frac{\epsilon}{\frac{4\epsilon' pc}{(mc^2)^2} (pc - \epsilon)}.$$

For simplicity, in the following we assume that the background radiation field is a black (grey) body, though these calculations may easily be extended to any background radiation spectrum. Depending on the environment we want to model, we consider either a single or a superposition of multiple Planck distributions, introducing a dilution factor η for each:

$$n(\epsilon') = \eta \frac{1}{\pi^2 \hbar^3 c^3} \frac{\epsilon'^2}{e^{\epsilon'/kT} - 1}, \quad (11)$$

where k is the Boltzmann constant and T the black body temperature.

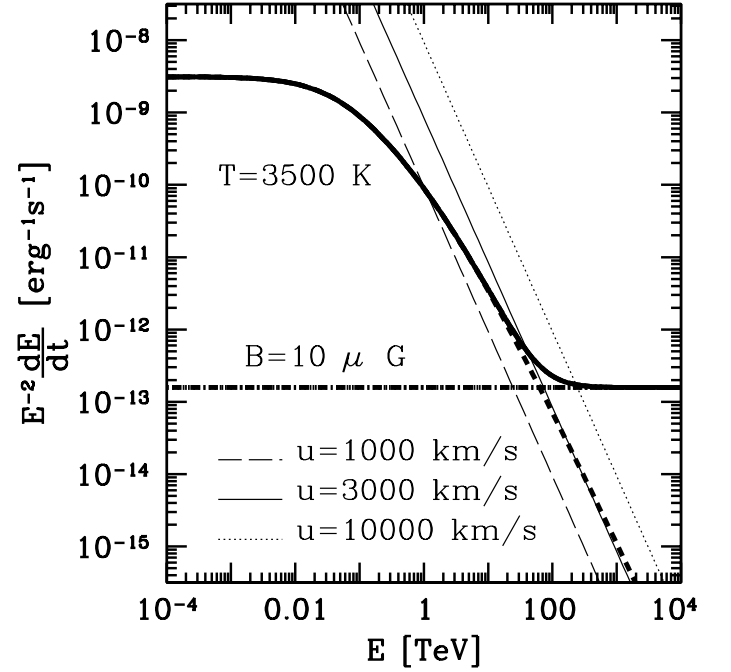


Fig. 1. Energy loss rates and shock acceleration rates for a magnetic field $B = 10 \mu\text{G}$ and a diluted black body radiation field at a temperature $T = 3500 \text{ K}$. All curves have been multiplied by E^{-2} so that Thomson losses correspond to horizontal lines. Thick lines: synchrotron loss rate (dot-dashed), inverse Compton loss rate (dashed) and the sum of the two (solid). Thin curves: acceleration rates for $u = 1000 \text{ km/s}$ (dashed), $u = 3000 \text{ km/s}$ (solid) and $u = 10000 \text{ km/s}$ (dotted).

3. Results

We present here the results of our calculation by means of an ideal case in order to illustrate the features and characteristics of the problem we are studying.

We consider a non-relativistic shock expanding in a medium where the magnetic field value is $B_1 = 10 \mu\text{G}$. Assuming a perfectly parallel shock, the magnetic field stays constant across the shock so that $B_2 = B_1$. For such a field, the magnetic energy density results $B^2/8\pi = 2.5 \text{ eV/cm}^3$. We assume that the accelerator is embedded in a background, isotropic, radiation field. We further assume a diluted black body radiation spectrum (i.e. with a reduced energy density) at a temperature of $kT = 0.3 \text{ eV}$ (i. e. in the Near Infrared energy band), corresponding to $T = 3500 \text{ K}$. We then assume the radiation energy density to be $U_{rad} = 5 \times 10^4 \text{ eV/cm}^3$, a factor 2×10^4 larger than the magnetic one (as we will point out in the next section, this high value is similar to the one measured in the $\leq 1 \text{ pc}$ Galactic Centre region (Davidson et al. 1992)).

In Fig. 1 we plot the energy loss rates contributed by synchrotron losses in a magnetic field of $10 \mu\text{G}$ (thick dot-dashed line) and by inverse Compton scattering off a radiation field at 3500 K (thick dashed curve), as a function of the particle energy. The sum of the two is represented by the thick solid curve. Also plotted in Fig. 1 are the acceleration rates for DSA in the same magnetic field and for three different values of the shock velocity ($u = 1000 \text{ km/s}$, dashed line, $u = 3000 \text{ km/s}$, solid line, and $u = 10000 \text{ km/s}$, dotted line). In this figure all curves have been multiplied by E^{-2} so that Thomson losses correspond to horizontal lines. The intersection between the acceleration rate curve and the total energy loss rate indicates the point in the

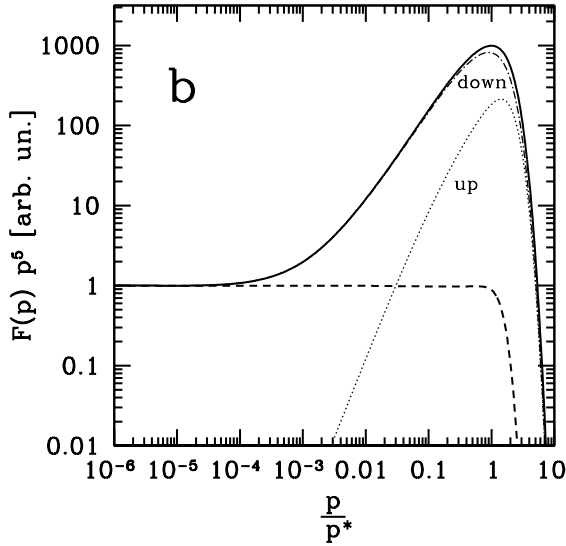
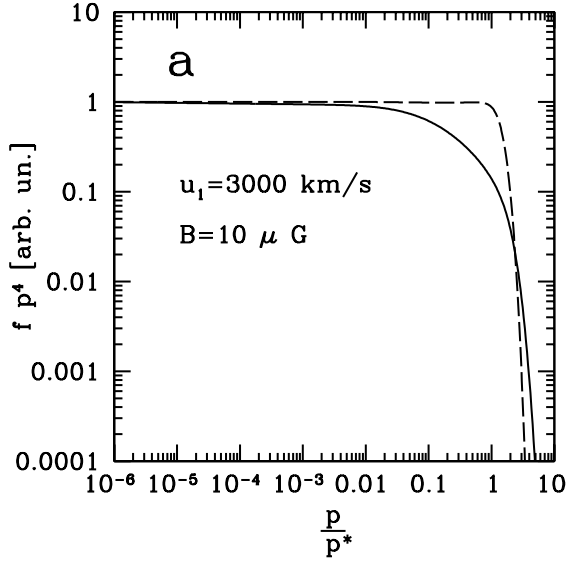


Fig. 2. a) Electron spectrum at the shock location in the case of inverse Compton dominated losses (solid line) and synchrotron cooling dominated case (dashed line) for a magnetic field $B = 10 \mu\text{G}$ equal up and downstream, shock velocity $u = 3000 \text{ km/s}$ and compression ratio $R = 4$. The background radiation field is assumed to be a diluted black body at $T = 3500 \text{ K}$ with energy density $U_{\text{rad}} = 5 \times 10^4 \text{ eV/cm}^3$. The momentum scale is normalized at the cutoff value p^* for each curve. The normalization on the y-axis is in arbitrary units. **b)** Electron distributions integrated over space. In the case of the IC dominated case (solid line) we also show separately the two components upstream (dotted) and downstream (dash-dotted). The dashed line represents the synchrotron dominated case.

particle energy spectrum where the acceleration due to DSA is compensated by radiative losses and therefore the cutoff sets in.

Fig. 1 shows how the energy dependence of energy losses changes behaviour. At low energies ($E \ll (mc^2)^2/\epsilon_{\text{ph}}$), inverse Compton proceeds in the Thomson regime ($dE/dt \propto E^2$), but at high energies the Klein–Nishina effect sets in, weakening the energy dependence of the process ($dE/dt \sim \ln E$). At even higher energies synchrotron losses become dominant and the Thomson regime is recovered.

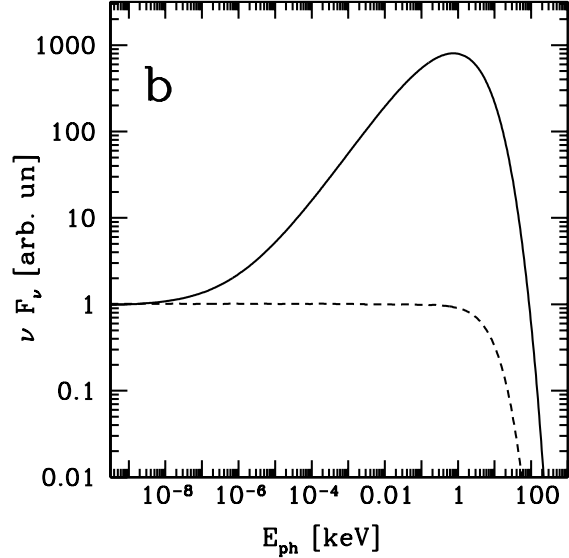
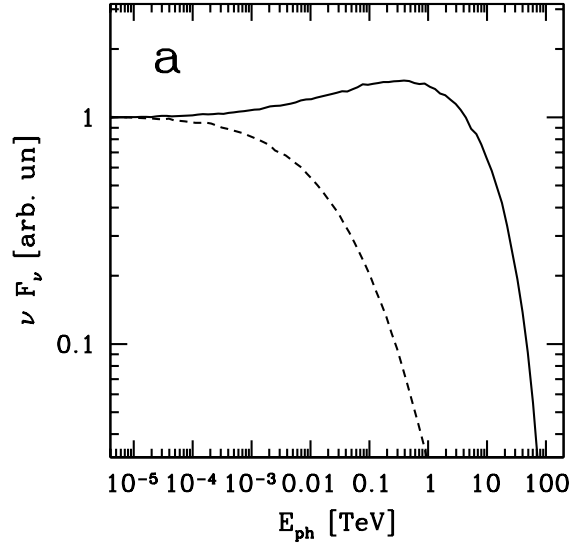


Fig. 3. a) Inverse Compton photon distribution produced by the electron spectra in Fig. 2b on a diluted black body at $T = 3500 \text{ K}$ for the case of dominant IC losses (solid line) and for the case of dominant synchrotron cooling (dashed line). **b)** Synchrotron emission from the two electron distributions in Fig. 2b, the magnetic field value is $10 \mu\text{G}$.

We solve the transport equation for the accelerated electrons choosing the value of 3000 km/s for the shock velocity. For such a choice of parameters, losses proceed deep in the KN regime. The shock is assumed to be strong, i.e. compression ratio $R = 4$, and we also assume a Bohm–like diffusion coefficient, namely $D = D_0 p^\beta$ with $\beta = 1$ and $D_0 = c^2/(3eB)$. The resulting electron energy spectrum at the shock location is shown in Fig. 2a (solid line). The dashed line, instead, shows the spectrum expected for the same values of the parameters but suppressing the radiation energy density (i.e. when synchrotron losses dominate). For an easier comparison we rescaled the momentum scale for each curve to its cutoff value p^* . Of course the actual value of p^* is different in the two cases. Note that the normalization on the y-axis is in arbitrary units. The solid curve shows that the shape of the spectrum is modified by the decrease of the IC cross-section at high energies: the cutoff region is broader and the decay is shallower, compared to the synchrotron case. The result may be

most easily understood from the rates in Fig. 1, which highlights the weak dependence on energy of Klein-Nishina losses.

To obtain the overall radiation produced by this population of electrons we have to consider the spatially integrated spectra $F_1 = \int_{-\infty}^0 f(x, p) dx$ and $F_2 = \int_0^{\infty} f(x, p) dx$. Fig. 2b shows the total spectrum $F(p) = F_1(p) + F_2(p)$ resulting from the integration for both cases of IC dominant losses (solid line) and of synchrotron dominant losses (dashed one). As can be seen, the most pronounced feature appears in the integrated spectrum: the softening of the losses causes a significant pile up around the cutoff energy (solid curve). For this case, we plotted also the upstream (dotted line) and downstream (dot-dashed line) distributions separately to show that the major contribution to the total spectrum is provided by the downstream distribution. In this region all particles are eventually advected away from the shock with the same velocity u_2 . The maximum distance to which they can actually propagate is determined by their loss length (while upstream it is essentially determined by diffusion). The loss length for each particle is $x_L = u_2 \tau_L$, where the loss time scale depends on the particle energy. In the first approximation, the particle integrated spectrum downstream can be written as $F_2(p) = f_0 x_L$. For Thomson scattering $\tau_L \propto E^{-1}$, determining that the higher the energy of the particle the smaller the distance it can travel away from the shock before losing its energy. For this reason the integrated spectrum in momentum space downstream results $\propto p^{-\alpha-1}$. In the case of KN losses we have an opposite trend: $\tau_L \propto E/\ln E$, so that high energy particles can propagate further than low energy ones and the resulting spectrum is harder. This effect produces the pile up when integrating the spectrum over space.

With the total spatially integrated spectrum obtained, we calculate the radiation emitted. Our results are shown in Fig. 3. Panel (a) shows the inverse Compton radiation resulting from the upscattering of the background radiation, when losses are Compton dominated (solid line), compared to the dominant synchrotron losses case (dashed line). The spectrum pile up is not so remarkable in the first case because the effect of the Klein-Nishina cross-section acts twice: while hardening the electron's distribution, it softens the IC photons' one, so that the two effects almost cancel each other.

On the other hand, the accelerated particles features have a sharp imprint on the synchrotron spectrum (Fig. 3b) which carries direct information on the electron distribution. Compared to the case of pure synchrotron cooling (dashed line), the emission due to an electron distribution shaped by IC losses (solid line) presents a pile up of three orders of magnitude around the cutoff, which, for the chosen parameters, appears at keV energies. This characteristic is a remarkable signature to distinguish the two different scenarios for electron radiative losses.

4. Applications

The results we obtained in the previous Section may have broad astrophysical application. To demonstrate this, we apply the results of our calculations to three specific astrophysical environments where strong non-relativistic shocks may form and in which the radiation energy density may dominate over the magnetic field energy density. The three cases we consider are: *i*) a supernova remnant in the Galactic Centre region, *ii*) the accretion shock surrounding clusters of galaxies and *iii*) a shock in a microquasar jet. For each of the considered cases, we evaluate both the electron spectrum and the spectrum of the emitted radiation.

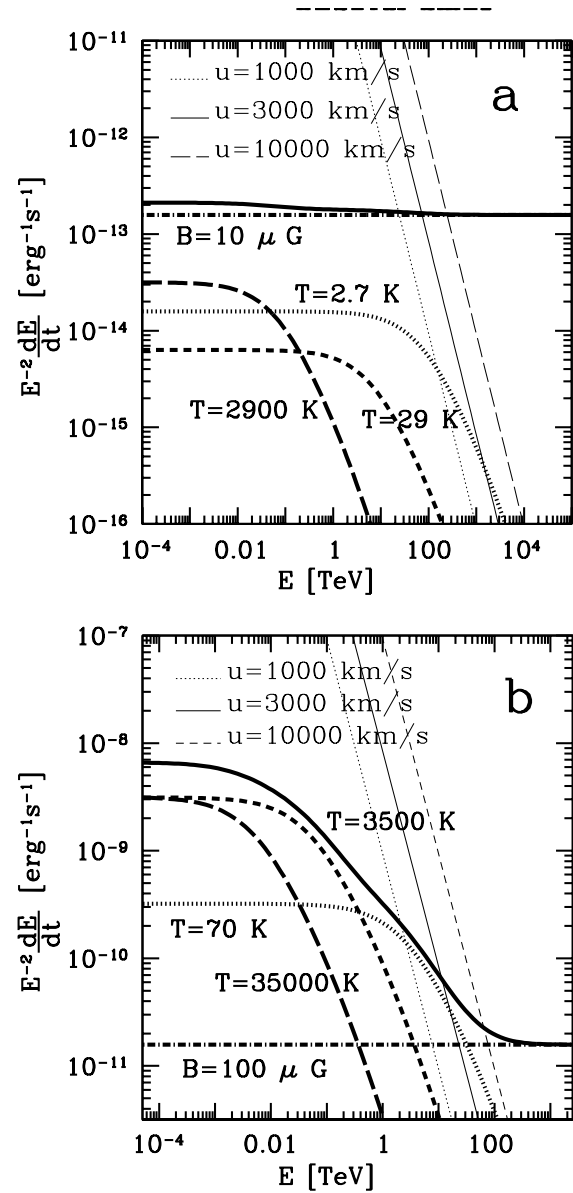


Fig. 4. a) Energy loss rates and acceleration rates, multiplied by E^{-2} , as a function of the electron energy E , for a Supernova Remnant in the Galactic Centre region. The synchrotron rate (thick dot-dashed line) corresponds to a magnetic field $B = 10 \mu\text{G}$, the IC curves are calculated for three black bodies at temperature $T = 2900 \text{ K}$ (Optical), thick long-dashed line; $T = 29 \text{ K}$ (Far Infrared), thick short-dashed line, and $T = 2.7 \text{ K}$ (CMB), thick dotted line. The thick solid curve represents the sum of the four loss contributions. Thin lines: acceleration rates for $B = 10 \mu\text{G}$ and shock velocity of 1000 km/s (dotted), 3000 km/s (solid) and 10000 km/s (dashed). **b)** Same as in panel a) but for a magnetic field of $100 \mu\text{G}$ and three black bodies at $T = 35000 \text{ K}$ (UV/Optical), $T = 3500 \text{ K}$ (NIR) and $T = 70 \text{ K}$ (FIR).

4.1. SNR in the Galactic Centre

Several observations in the radio and X-ray bands have confirmed Supernova Remnants (SNR) shocks as powerful accelerators of electrons up to tens of TeV (Bamba et al. 2003). We first consider a SNR in the galactic disk. The radiation field in the Galaxy consists of three distinct components: the optical/Near-Infrared (NIR), the Far Infrared (FIR) and the

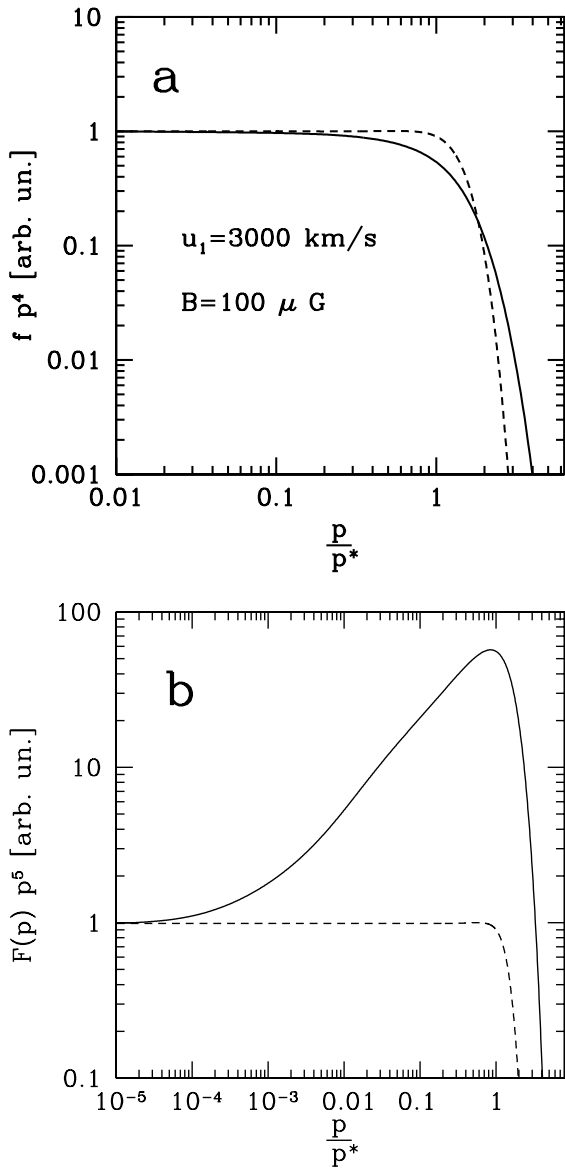


Fig. 5. **a)** Electron spectrum at the shock for a velocity of 3000 km/s and a magnetic field $B = 100 \mu\text{G}$. The solid line is obtained in the case of dominant IC losses with the same parameters as in Fig. 4b, the dashed line corresponds to the case when the radiation energy density is suppressed and synchrotron cooling dominates. **b)** Integrated spectra for same values of the parameters of panel (a).

Cosmic Microwave Background (CMB) radiation, with an energy density of $\sim 0.5, \sim 0.1, \sim 0.25 \text{ eV/cm}^3$ respectively (Mathis et al. 1983). In our calculation we evaluated an effective temperature for these fields from their peak energy and then assumed they can be approximated with a diluted black body distribution. The Galactic magnetic field has a measured value of $\sim 3 \mu\text{G}$ (see Widrow 2002 for a review), which corresponds to an energy density of $\sim 0.23 \text{ eV/cm}^3$. This implies that the average magnetic field energy density is comparable to the radiation one. Moreover, the magnetic field can be significantly amplified in the presence of a shock which is efficiently accelerating particles (Bell & Lucek 2001), so that, in the acceleration region, results $U_{\text{mag}} \gg U_{\text{rad}}$. Therefore synchrotron losses are dominant over inverse Compton (Fig. 4a). In this case the con-

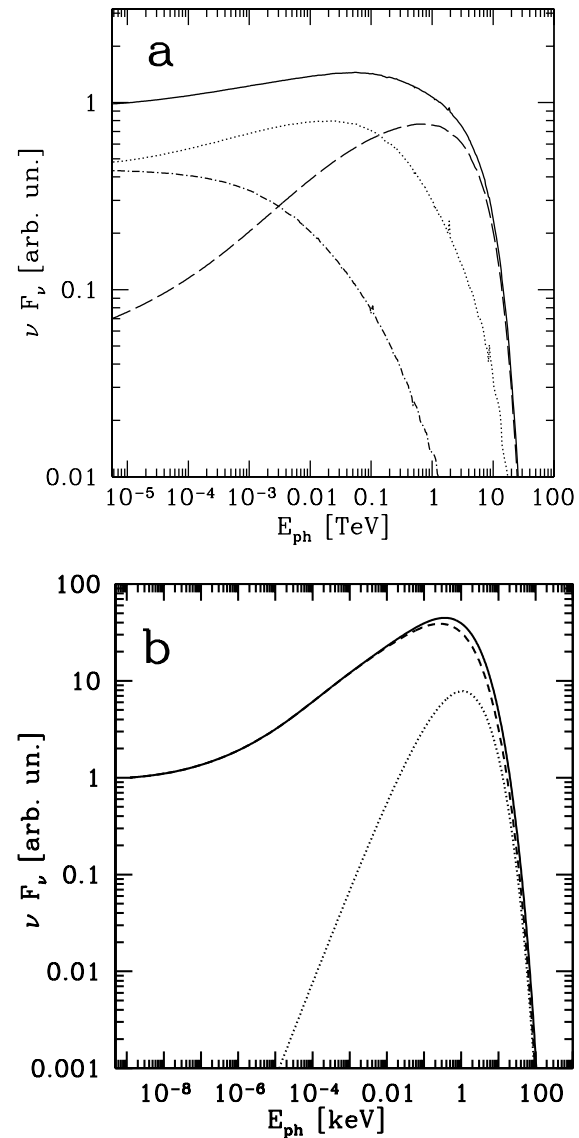


Fig. 6. Radiation emitted by the electron distribution in Fig. 5b, solid line. **a)** total inverse Compton spectrum (solid line) from the three background radiation components: FIR (dashed), NIR (dotted) and UV/Optical (dot-dashed). **b)** Synchrotron radiation produced in the downstream (dashed) and upstream (dotted) regions, together with the sum of the two (solid line); the value of the magnetic field is $100 \mu\text{G}$.

tribution of the IC to the energy loss rate is negligible and the cutoff energy and shape are determined by synchrotron cooling.

Things are dramatically changed, though, if we consider a SNR in the Galactic Centre (GC) region, where both the magnetic and the radiation fields are much stronger than the average Galactic values. In analogy with what done in Hinton & Aharonian (2007), we consider the inner 1 pc of the Galaxy, where the values of the radiation energy density are $5 \times 10^4 \text{ eV/cm}^3$ at $kT = 3.0 \text{ eV}$ (UV) and $kT = 0.3 \text{ eV}$ (NIR), and $5 \times 10^3 \text{ eV/cm}^3$ at $kT = 6 \times 10^{-3} \text{ eV}$ (FIR) (Davidson et al. 1992). To have an equal energy density in the magnetic field it is required that $B \approx 500 \mu\text{G}$, any lower value implies the dominance of IC (KN regime) losses in determining the cutoff of the electron spectrum. We choose $B = 100 \mu\text{G}$

As shown in the Fig. 4b, for a velocity of 3000 km/s and a magnetic field of $100 \mu\text{G}$, the cutoff energy results $E^* \approx 10 \text{ TeV}$.

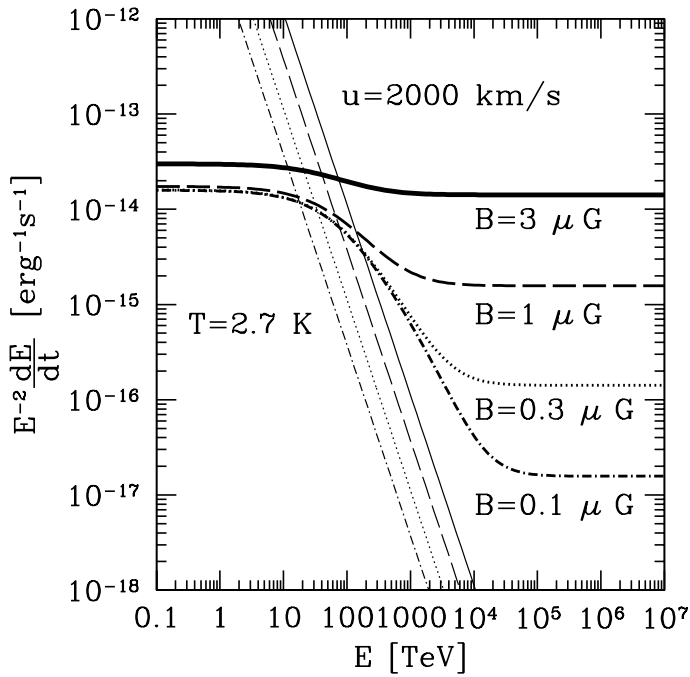


Fig. 7. The thick lines represent the energy loss rates (synchrotron plus IC) for typical conditions in a galaxy cluster’s accretion shock: the background radiation field is provided by the CMB and the values of the magnetic field are reported. The thin lines represent acceleration rates for a shock velocity of 2000 km/s and the line type refers to the corresponding value of B .

Considering these values for the shock velocity and the magnetic field we calculate the spectrum at the shock ($x = 0$). The result is shown in Fig. 5a (solid line), where we compare it with the one obtained for pure synchrotron losses, with the same values of the other parameters (dashed line). The features are those pointed out in Section 3: the cutoff region is broader and the decay is less steep than for synchrotron cooled electrons.

In Fig. 5b we plot again the spatially integrated spectra for the two cases of IC (solid) and synchrotron (dashed) dominated losses. For both curves the up and downstream contributions have been summed up. Here the modification of the spectrum due to KN effects can be dramatic. In our example the hardening of the spectrum right below the cutoff causes a pile up of about two orders of magnitude, compared with the case of dominant synchrotron losses.

Once we have the electron spectrum we can calculate the photon distribution. Fig. 6a shows our results for IC: we plot the spectra for the three different components of the seed field (FIR, NIR, UV) as well as their sum. The overall radiation spectrum shows an almost flat profile below the cutoff due to the compensation of the “double action” of Klein-Nishina effect. The situation is different for the synchrotron emission. We plot in Fig. 6b the spectrum in its two components, downstream and upstream, as well as their sum. As expected a pronounced pile up feature appears around the cutoff energy.

4.2. Clusters of Galaxies

Another example of a radiation dominated environment where a shock can form is represented by clusters of galaxies. Rich clusters of galaxies are the biggest virialized structures in the Universe, with typical sizes of a few Mpc and masses up to

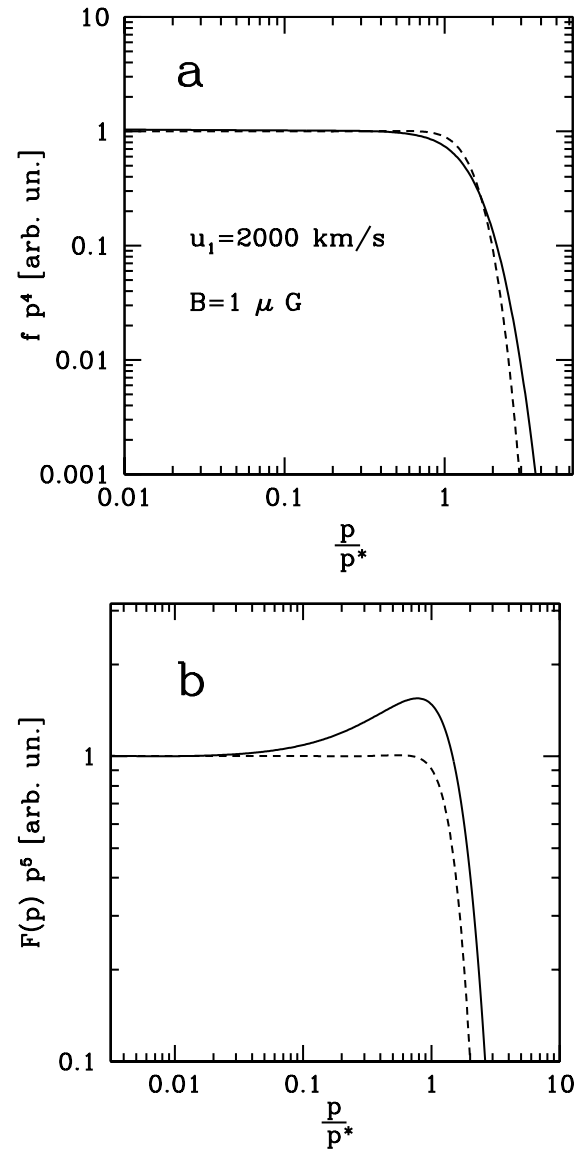


Fig. 8. a) Electron distribution at the shock front for a shock velocity of 2000 km/s and a magnetic field of $1 \mu\text{G}$ in the two cases of intense inverse Compton losses (solid line) and dominant synchrotron cooling. **b)** Integrated spectra for IC dominated case (solid) and synchrotron dominated case (dashed).

$10^{15} M_{\odot}$ or more (see Sarazin 1988 for a review). An expanding shock wave, called the accretion shock, forms at the cluster boundary and carries outward the information of virialization (Bertschinger 1985). The infalling matter crosses the shock surface at a speed roughly comparable to the free fall velocity, namely:

$$v_s \sim \sqrt{\frac{2GM_{cl}}{R_{cl}}} \approx 2000 \left(\frac{M_{cl}}{10^{15} M_{\odot}} \right)^{1/2} \left(\frac{R_{cl}}{3 \text{ Mpc}} \right)^{-1/2} \text{ km/s}$$

so that the shock velocities are comparable to the one found in supernova remnants. Particle acceleration is expected to happen at accretion shocks (see Blasi et al. 2007 for a review) with consequent emission of inverse Compton gamma rays, possibly detectable in the near future by GLAST or ground based Cherenkov telescopes (Gabici & Blasi 2004).

The detection of a tenuous and diffuse synchrotron radio emission from about one third of rich clusters of galaxies

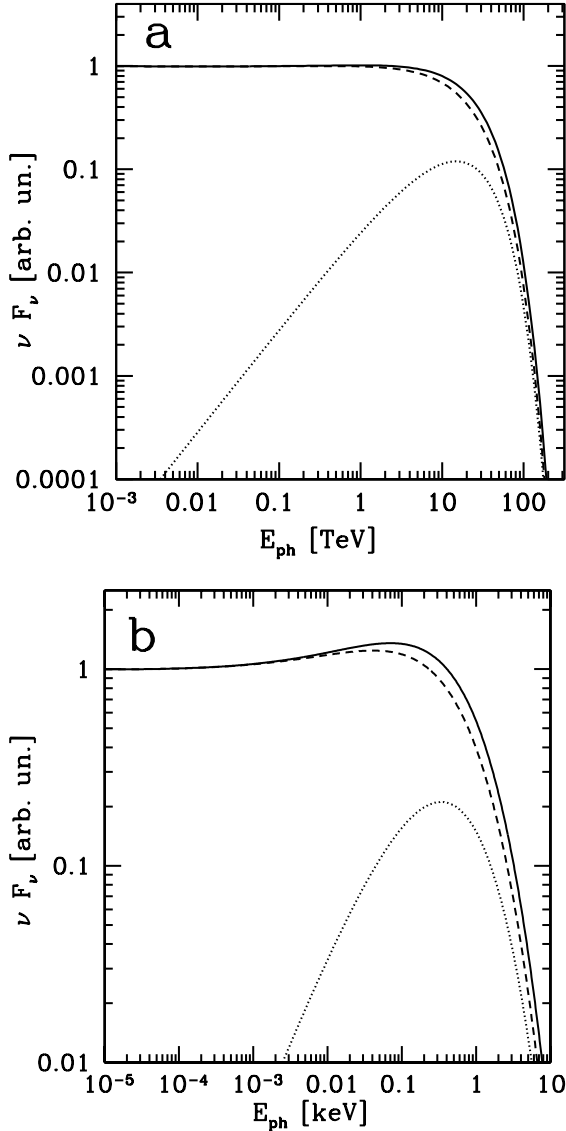


Fig. 9. **a)** Inverse Compton spectrum produced by upscattering of the CMB for the distributions in Fig 8b. The dashed line shows the downstream contribution, the dotted the upstream one. The solid line is the sum of the two. **b)** The dotted line shows the synchrotron radiation emitted in the upstream region, the dashed one the downstream region and the solid one their sum for a magnetic field value of $B = 1 \mu\text{G}$

(Feretti & Johnston-Hollitt 2004; Carilli & Taylor 2002) reveals the presence of a magnetic field of the order of few μG in the intracluster medium. The value of the magnetic field in the cluster outskirts, where the accretion shock propagates, is unknown, due to lack of radio measurements, but it is likely to be smaller or at most comparable with the one measured in the inner regions. Thus, the magnetic field energy density at the shock position is $\sim 0.025 \text{ eV}/\text{cm}^3$ for $1 \mu\text{G}$ magnetic field. This implies that at the position of the shock the main energy loss channel for relativistic electrons is inverse Compton scattering in the Cosmic Microwave Background photon field, characterized by an energy density of $\sim 0.25 \text{ eV}/\text{cm}^3$. Optical and infrared radiation from cluster galaxies is totally negligible.

In Fig. 7 we plot the energy loss rates for a “typical” galaxy cluster. The thin lines represent the acceleration rates for a velocity $u = 2000 \text{ km/s}$ and different values of the magnetic field. The

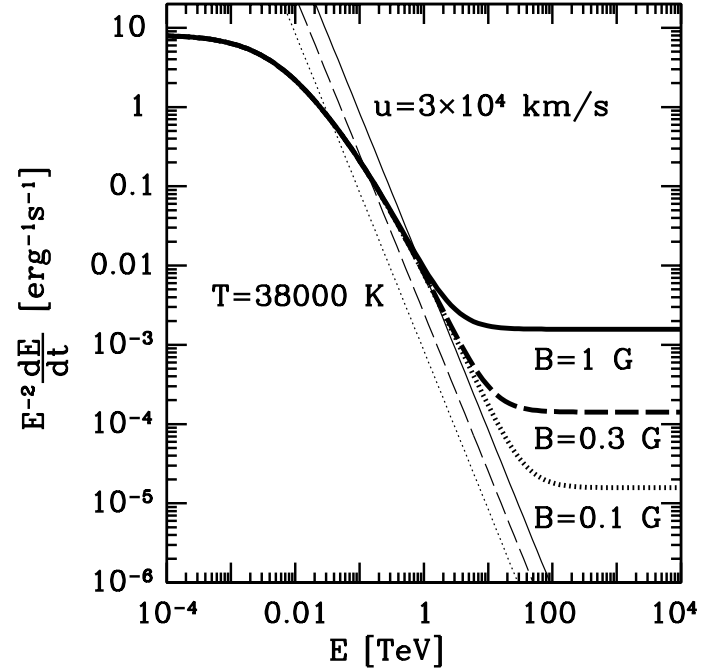


Fig. 10. Total loss rates (thick lines) due to IC upscattering of the star photon field at $kT \approx 3.3 \text{ eV}$ plus synchrotron emission for the values of B reported, feasible for a Microquasar. The shock velocity is fixed at 30000 km/s and the thin lines correspond to the acceleration rates connected to the values of the magnetic field for which we plot the loss rates.

thick lines are the total energy loss rates for inverse Compton scattering off the CMB plus synchrotron emission. Calculations are done for four values of the magnetic field: $3 \mu\text{G}$ (solid lines), $1 \mu\text{G}$ (dashed), $0.3 \mu\text{G}$ (dotted) and $0.1 \mu\text{G}$ (dot-dashed).

Below we consider the case of parameter values: $B = 1 \mu\text{G}$ and $u = 2000 \text{ km/s}$, reasonable for an accretion shock around a rich cluster (Blasi et al. 2007). In this case, the cutoff energy falls in the KN dominated part of the total loss rate, at about 70 TeV (corresponding to the intersecting point between the thick dashed line and the thin dashed line in Fig. 7).

In Fig. 8a we plot the electron spectrum at the shock (solid line), compared to the one expected for pure synchrotron losses (dashed line). The modification due to the dominant IC losses is less pronounced than in the Galactic Centre case considered in Section 4.1, as expected from Fig. 7, but the characteristics are the same as those noticed before: a wider and less sharp cutoff.

If we look at the effect this produces on the total spatially integrated particle spectrum, we find a pile up of a factor ~ 2 around the cutoff energy (Fig. 8b).

The photon spectra are affected in a similar way. In Fig. 9a we plot the upscattered spectrum of the CMB. We plot the two contributions to the total spectrum from the upstream (dotted) and downstream (dashed) regions, the latter dominating the total spectrum. Fig. 9b shows the synchrotron spectrum where the pile up feature of the electron spectrum is reproduced.

4.3. Microquasars

Another class of objects of great interest are the Microquasars. These are galactic binary systems composed of a regular O/B star being accreted onto a compact object (neutron star or black hole) that presents a jet.

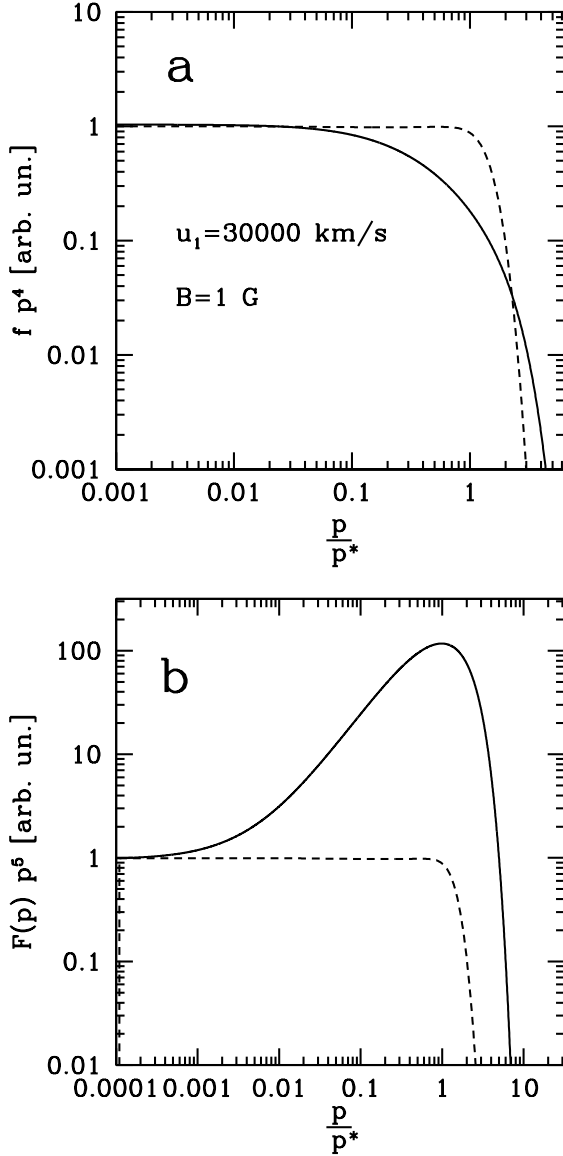


Fig. 11. **a)** Electron spectrum at the shock for a shock velocity $u = 30000$ km/s. The value of the magnetic field is $B = 1$ G and the solid line represent the case of dominant IC losses, while the dashed one is obtain with pure synchrotron cooling. **b)** Integrated electron spectra for the two cases in plot (a).

The nature of these objects is very complex and is not yet fully understood. Nevertheless the basic ingredients present in the system are a very intense stellar radiation field (e.g. for LS 5039 the luminosity of the star is $L_* \simeq 7 \times 10^{38}$ erg/s implying a radiation energy density up to $U_{rad} \simeq 1000$ erg/cm³, depending on the location, at a temperature of $T \simeq 3.8 \times 10^4$ K (Casares et al. 2005)) and a jet which is thought to be the site of particle acceleration. If blobs of plasma are emitted in the jet at slightly different velocity, internal sub-relativistic shocks can form, where electrons acceleration can take place. The value of the magnetic field is not known, but with reasonable range between 0.01 and 1 G.

For our calculation we refer to the model used in Khangulyan et al. (2007), where the jet from the compact object is assumed to have the axis perpendicular to the orbital plane and we put the acceleration zone at a distance $Z_0 = 2 \times 10^{12}$ cm from the jet base (this corresponds to a distance equal to the mean

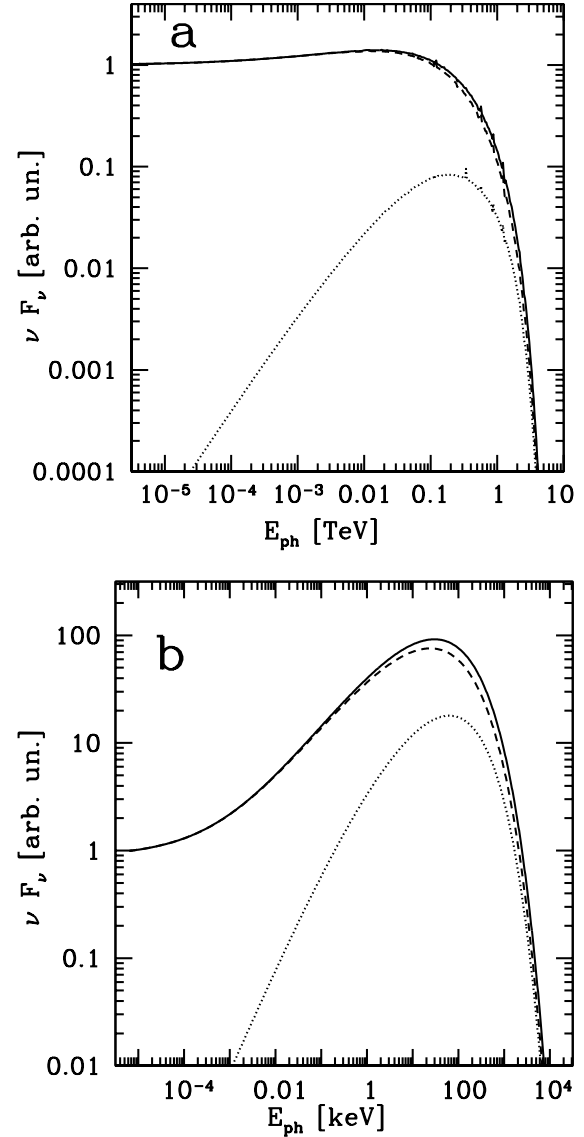


Fig. 12. Photon spectrum produced by the electron spectrum represented by the solid line in Fig. 11b. **a)** IC spectrum for a diluted black body of temperature $T \simeq 3.8 \times 10^4$ K. The dashed line shows the downstream contribution, the dotted one the upstream. The solid line is the sum of the two. **b)** Synchrotron spectrum for $B = 1$ G produced upstream (dotted), downstream (dashed) and the sum of the two (solid).

orbital radius). At such a distance the radiation energy density results:

$$\frac{L_*}{4\pi c(R_{orb}^2 + Z_0^2)} \simeq 230 \frac{erg}{s} \quad (12)$$

In Fig. 10 we plot as thick lines the total energy loss rates due to IC plus synchrotron losses and as thin lines the acceleration rates for a shock velocity of 30000 km/s. The solid lines correspond to a magnetic field value of 1 G, the dashed ones to $B = 0.3$ G and the dotted lines to $B = 0.1$ G. We chose $u = 30000$ km/s, corresponding to 10% of the speed of light, in order to be still consistent with the assumption of non-relativistic shock.

In this case the radiation energy density is considerably bigger than the magnetic one also for a field $B = 1$ G. This is the

value we will consider in our calculation in order to obtain an efficient acceleration of electrons up to TeV energies. Moreover, from a theoretical point of view, this choice allows us to explore a different region of the KN losses, compared with the previous two cases.

In Fig. 11a and 11b we plot the electron spectrum at the shock and integrated over space. In this case the predominance of the IC is such that the hardening of the spectrum is very pronounced (solid line). The pile up is two orders of magnitude above the synchrotron case (dashed line).

As in the previous cases, the IC photon spectrum doesn't show prominent features (Fig. 12a), while the synchrotron one reproduces the electron pile up (Fig. 12b).

5. Conclusions

In this paper we have addressed the problem of particle acceleration at non-relativistic shocks in the presence of strong energy losses, specifically in the case, never treated before, of electrons undergoing severe inverse Compton losses in the Klein-Nishina regime.

We solved numerically the complete transport equation for the accelerated particles and calculated the particle distribution function $f(x, p)$ and the resulting radiation spectra.

Our approach provides a general tool for what concerns the species of particles accelerated (electrons and protons), the type of losses and the form of the diffusion coefficient. In this work we focused on electrons undergoing synchrotron and inverse Compton losses, in the case where the radiation energy density is larger than the magnetic one. We assumed Bohm diffusion: $D(p) = pc^2/(3eB)$.

For high energy electrons, with energy $E \geq (mc^2)^2/\epsilon_{ph}$, the inverse Compton scattering enters the Klein-Nishina regime where the cross-section decreases with energy. We evaluated the particle spectrum at the shock and found that, compared to the case of Thomson losses, the KN effect results in a broadening of the cutoff region and a hardening of the spectrum around the cutoff energy. The latter effect is most evident in the spatially integrated spectrum, which exhibits a pronounced pile up feature just below the cutoff energy. Such a feature can be significant, with an enhancement of the spectrum up to a few orders of magnitude, depending on the ratio of energy densities U_{rad}/U_{mag} , the magnetic field strength and the shock velocity.

Once the electron spectrum is obtained, we can calculate the resulting spectra of the radiation, both synchrotron and inverse Compton. The hardening in the electron spectrum is almost not visible at all in the IC spectrum since the effect of the KN cross-section on the scattering process itself compensates the opposite action on the electron spectrum. The pile up feature is reproduced by the synchrotron distribution, which no longer follows a simple power law below the cutoff, as in the case of dominant Thomson losses.

We demonstrated the importance of this effect in three examples of astrophysical objects in which the energy density of the radiation field dominates over the magnetic field energy density, namely a Supernova located in the Galactic Centre region, the accretion shocks of clusters of galaxies and the internal shocks in the jet of a Microquasar, and discussed the possible consequences of our results on the emission of these objects.

Acknowledgements. We especially thank V. Zirakashvili for all the useful advice and suggestions. We would also like to acknowledge A. M. Taylor, D. Khangulyan, V. Bosch-Ramon and B. Reville for fruitful discussions. GV acknowledges support from the International Max-Planck Research School

(IMPRS) Heidelberg. SG acknowledges the support of the European Community under a Marie Curie Intra-European fellowship.

References

- Bamba, A., Yamazaki, R., Ueno, M., Koyama, K. 2003, *ApJ*, 589, 827
 Bell, A.R., Lucek, S.G. 2001, *MNRAS*, 321, 433
 Bertschinger, E. 1985, *ApJ Suppl.*, 58, 39
 Blandford, R.D., Eichler, D. 1987, *Phys. Rep.*, 154, 1
 Blasi, P., Gabici, S., Brunetti, G. 2007, *astro-ph/0701545*
 Blumenthal, G.R., Gould, R.J. 1970, *Rev. Mod. Phys.*, 42, 237
 Bulanov, S.V., Dogiel, V.A. 1979, *Sov. Astron. Letters*, 5, 278
 Carilli, C.L., Taylor, G.B. 2002, *ApJ*, 577, 22
 Casares, J., Ribó, M., Ribas, I., Paredes, J.M., Martí, J., Herrero, A. 2005, *MNRAS*, 364, 899
 Crusius, A., Schlickeiser, R. 1986 *A&A*, 164, L16
 Davidson, J.A., Werner, M.W., Wu, X., Lester, D.F., Harvey, P.M., Joy, M., Morris, M. 1992, *ApJ*, 387, 189
 Feretti, L., Johnston-Hollitt, M. 2004, *New Astr. Rev.*, 48, 1145
 Gabici, S., Blasi, P. 2004, *Aph*, 30, 579
 Heavens, A.F., Meisenheimer, K. 1987, *MNRAS*, 225, 335
 Hinton, J.A., Aharonian, F.A. 2007, *ApJ*, 657, 302
 Khangulyan, D., Aharonian, F.A., Bosch-Ramon, V. 2007, *ArXiv0707.1689*
 Malkov, M.A., Drury L.O'C. 2001, *Rep. Prog. Phys.*, 64, 429
 Mathis, J.S., Mezger, P.G., Panagia, N. 1983, *A&A*, 128, 212
 Sarazin, C.L. 1988, *X-ray Emission from Clusters of Galaxies*, Cambridge University Press, i-x,1-252
 Webb, G.M., Drury, L.O'C., Biermann, P. 1984, *A&A*, 137, 185
 Widrow, L.M. 2002, *RvMP*, 74, 775.
 Zirakashvili, V.N., Aharonian, F.A. 2007, *A&A*, 465, 695